Thermochimica Acta 473 (2008) 32–39

Contents lists available at ScienceDirect

Thermochimica Acta

journal homepage: www.elsevier.com/locate/tca

Numerical modelling of the adsorption and thermal desorption of NH_3 on ZrO_2

T. Finke [a,b,*], M. Gernsbeck [a], U. Eisele [a], C. Vincent [a], M. Hartmann [b], S. Kureti [b], H. Bockhorn [b]

[a] Robert Bosch GmbH, Corporate Sector Research and Advance Engineering, Postal Box 106050, Stuttgart D-70049, Germany
[b] University of Karlsruhe, Institute of Technical Chemistry and Polymer Chemistry, Karlsruhe D-76128, Germany

ARTICLE INFO

Article history:
Received 29 January 2008
Received in revised form 6 April 2008
Accepted 10 April 2008
Available online 21 May 2008

Keywords:
Numerical modelling
TPD
DRIFTS
ZrO_2
NH_3
Activation energy

ABSTRACT

This paper deals with the interaction of NH_3 with ZrO_2. The adsorption sites of the ZrO_2 surface and the thermal behaviour of the adsorbates formed are examined by Diffuse Reflectance Infrared Fourier Transform Spectroscopy (DRIFTS). Kinetic parameters of the adsorption and desorption of NH_3 are determined by numerical modelling based on Temperature Programmed Desorption (TPD) studies. Special interest was directed towards TPD spectra, which exhibited an intense peak in the low-temperature range as well as a sample dependent shoulder at higher temperatures corresponding to $H_3N\cdots\cdots HO–Zr^{4+}$ and $H_3N\cdots\cdots Zr^{4+}$ surface species, respectively. Kinetic modelling provided activation energies for NH_3 desorption between 100 and 105 kJ mol^{-1} and from 141 to 164 kJ mol^{-1}.

1. Introduction

The emission of nitrogen oxides (NO_x), carbon monoxide (CO) and hydrocarbons (HC) is predominately caused by combustion of fossil fuels, waste and further organic energy sources like timber. In gasoline engine systems these pollutants are reduced by the use of Pt/Rh or Pd/Rh containing three-way catalysts (TWC). However, this simultaneous conversion occurs exclusively within a narrow range of O_2 content that is close to stoichiometric combustion conditions, i.e. when the excess-air coefficient λ ranges from 0.99 to 1.01 [1]. Thus, the lambda sensor, which was introduced into the market in 1976, is of particular concern for TWC applications. The sensor measures the λ coefficient present in the exhaust stream forcing the engine management system to regulate fuel injection.

Lambda sensors applied in gasoline systems are composed of a material with specific conductivity, for instance Pt, as well as a ceramic component exhibiting oxygen ion conductivity, e.g. yttrium stabilised zirconia (YSZ). For the production of the latter the physical–chemical properties of respective YSZ powder batches play an important role because of decisively affecting the whole manufacturing process as well as the quality of the end-product. However, for the optimisation of the production steps classical approaches are considered to be problematic for modern R&D requirements as they include empiric and time consuming methodologies. In contrast to that, the characterisation and evaluation of specific surface-chemical and adsorption properties of the ceramic precursors should allow a direct process design on a molecular level, thus representing a powerful tool for sustainable development as well as production improvements. Moreover, it should be noticed that defined physical–chemical properties of ZrO_2 materials are also crucial for other potential applications, e.g. for catalysis [2,3].

Various procedures are known from the literature to determine thermodynamic and kinetic parameters of the adsorption and desorption of gases on oxide systems [4]. Gerasini et al. report on microcalorimetric methods for the evaluation of adsorption enthalpies [5–8], while Makowski, Kanervo, Panczyk, and Keskitalo et al. use Temperature Programmed Desorption (TPD) analysis for determining adsorption enthalpies by methods based on quasi-equilibrium assumptions [4,9–12]. Additionally, TPD techniques are used to calculate activation energies for desorption reactions of gases according to the procedure proposed by Redhead (Eq. (1)) [13].

$$\frac{E_a}{RT_{max}} = \ln\frac{\upsilon_1 T_{max}}{\beta} - 3.64 \quad (1)$$

E_a: activation energy of desorption, R: ideal gas constant, T_{max}: temperature of the concentration maximum of TPD pattern, υ_1: preexponential Arrhenius factor, β: heating rate.

* Corresponding author at: Robert Bosch GmbH, Corporate Sector Research and Advance Engineering, Postal Box 106050, Stuttgart D-70049, Germany. Tel.: +49 711 811 38367; fax: +49 711 811 5181605.
E-mail address: thomas.finke2@de.bosch.com (T. Finke).

0040-6031/$ – see front matter © 2008 Elsevier B.V. All rights reserved.
doi:10.1016/j.tca.2008.04.006

Furthermore, Smith and Aranoff and Ehrlich describe the "flash-filament" method for determining activation energies and reaction orders of adsorption and desorption processes [14,15].

All activation energy calculating techniques mentioned above refer to symmetric desorption signals only. Thus, detailed analysis of asymmetric TPD patterns involving the superposition of desorption signals is problematic.

Sato et al. report on the deconvolution of asymmetric TPD profiles by using Gaussian curves defining T_{max} and the ratio of the corresponding adsorption sites [16]. However, kinetic and thermodynamic aspects of respective elementary reactions are not taken into account. Further examples of processing multi-peak TPD patterns by fitting one desorption peak followed by subtracting it from the total TPD curve are given in the literature [17,18]. These methods do not obey the principle of free readsorption because the subtraction corrupts information regarding gas-phase compositions.

Contrary, Zhdanov and Matsushima describe calculations of complex TPD patterns using Kinetic Monte Carlo simulations [19,20]. Theoretical basics of kinetic Monte Carlo simulations are discussed in [21,22].

In this work we present detailed characterisation of the surface sites of YSZ and ZrO_2 samples which is expected to be a key for the optimisation of process parameters and future development lines of sensor materials. For this purpose NH_3 is taken as probe molecule, while the surface complexes formed are analysed with Diffuse Reflectance Infrared Fourier Transform Spectroscopy (DRIFTS) and TPD. A kinetic model, which describes the adsorption/desorption equilibrium on specific surface sites using elementary reactions is constructed by combination of DRIFTS and TPD data. Corresponding kinetic parameters are obtained by numerical modelling of the asymmetric NH_3 TPD patterns.

2. Experimental

2.1. Materials

In the present study four model patterns are investigated (Table 1).

Table 1
Physical characteristics of the materials used

Sample	$m(Y_2O_3)$/wt.%	S_{BET}/m^2 g^{-1}	d_{50}/nm
YSZ-A	6.5	11.6	347
YSZ-B	6.5	11.8	350
NYSZ	5.4	64.2	25
NZ	–	155	20

YSZ-A and YSZ-B are sub-μ-scaled yttrium doped zirconia samples, which are produced by melting ZrO_2 and Y_2O_3 in an electric arc furnace and finely milling the doped oxide gained. They exhibit a Y_2O_3 content of 6.5 wt.% and a specific surface area of 11.6 and 11.8 m^2 g^{-1}, respectively. Nano-sized YSZ (NYSZ) is a highly dispersed zirconia (d_{50}: 25 nm) which is gained within an Aerosil® process by high temperature pyrolysis of a metal organic precursor [23]. The sample reveals good chemical (impureness <0.05%) and crystallographic (>99% monoclinic) purity. The Y_2O_3 content is 5.4 wt.%, while the BET surface area amounts to 64.2 m^2 g^{-1}. NZ is an undoped nano-zirconia which is synthesised in a precipitation process, exhibiting a specific surface area of 155 m^2 g^{-1} and a d_{50} of 20 nm.

2.2. TPD studies

The setup used for TPD and DRIFTS experiments consists of five integral components, i.e. gas supply, TPD system, surface analytics, gas analytics and system control (Fig. 1).

Thermal mass flow controllers (MKS Instruments, Munich) are used for gas dosage. The setup additionally allows in situ characterisation of the temperature dependence of heterogeneous reactions and adsorption processes of organic components onto various matrices, e.g. ceramics and catalysts. For this purpose liquids are fed into an evaporating system using a μ-LiquiFlow (Bronkhorst, Ruurlo). The vapour is subsequently injected into the gas supply system.

Stainless steel pipes are passivated by Restek Performance Coatings (Bellefonte) for the quantitative transfer of the gas molecules from the plug flow reactor (quartz glass tube; i.d.: 22 mm; length: 750 mm) to the gas analytics. Chemical inert Siltek®/Sufiniert® pas-

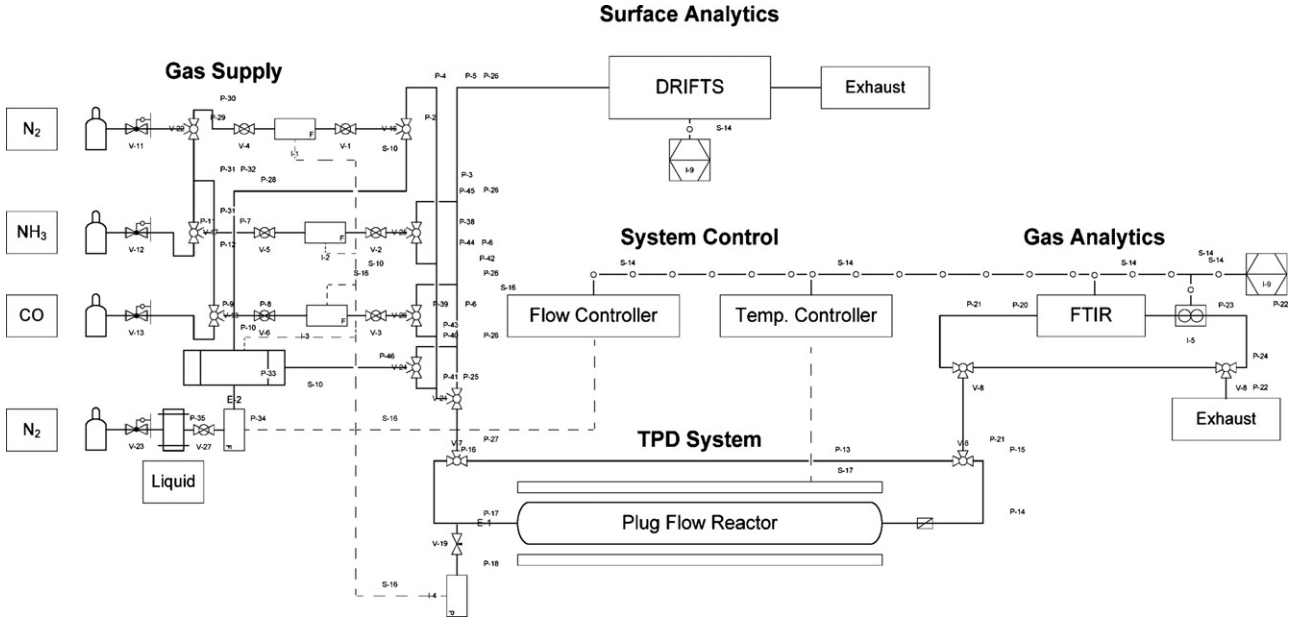

Fig. 1. Scheme of the analytical bench used.

sivation minimises adsorption and readsorption effects of active components on the tubes.

Simultaneous realisation of TPD and DRIFTS analysis is feasible due to the possible combinations of separate gas and vapour flows.

The bench described is considered to be an effective alternative compared to other TPD setups reported in literature [24–29]. TPD analyses are performed without thermal pre-treatment of the samples to examine surface-chemical characteristics and adsorptions properties which are relevant for industrial batch-processing. The powders (YSZ-A/YSZ-B: 5.0 g; NYSZ: 1.0 g; NZ: 0.8 g) are purged in the plug flow reactor with dry N_2 for 1 h at 25 °C to remove adsorbed species, i.e. mainly H_2O. After this, the respective solid is treated with a gas mixture of 500 ppm NH_3 in N_2 at a flow of 1.00 l min^{-1} (STP) until the saturation equilibrium is reached. NH_3 is considered to be a useful probe molecule for the surface characterisation of ZrO_2 samples due to its dosage ability and specific reactivity towards Lewis and Brønsted acid sites [30]. Subsequently, the sample is flushed with N_2 to remove physisorbed NH_3. TPD is started using N_2 as carrier gas (1.00 l min^{-1}, STP) and a linear heating rate of 15 K min^{-1} up to 550 °C. The reactor effluents are continuously monitored by FTIR spectroscopy (PerkinElmer 1720X equipped with a 200 ml gas cell; path length: 3.6 m).

2.3. DRIFTS studies

DRIFTS examinations are performed on a Bruker Equinox 55 FTIR equipped with a MCT detector and praying mantis optics from Harrick. The stainless steel IR cell contains KBr windows and is connected to a gas-handling system. The temperature is monitored by a K-type thermocouple placed 7 mm underneath the sample surface. During measurements the spectrometer as well as the DRIFTS optics are purged with N_2 to avoid diffusion of air into the system. The spectra are recorded in the range from 500 to 4000 cm^{-1} with an instrument resolution of 4 cm^{-1}. 100 scans are accumulated to a spectrum using a KBr background. All spectra are displayed in the Kubelka–Munk function (Eq. (2)) providing linear interrelation between the band intensity and the sample concentration, improved base line progression and better resolution [31,32].

$$F(R) = \frac{(1-R)^2}{2R} = \frac{\varepsilon \cdot c}{s} \quad (2)$$

s: grain size dependent dispersion coefficient, ε: decadal extinction coefficient, c: concentration.

The relative reflectivity R is defined as the ratio of the reflectance of the sample I and that of the KBr reference I_0 (Eq. (3)).

$$R = \frac{I}{I_0} \quad (3)$$

The Kubelka–Munk relation equals the Beer–Lambert Law of the transmission spectroscopy and allows quantitative analysis of the diffuse reflectance spectroscopy.

2.4. Calculation of kinetic parameters of NH_3 adsorption/desorption reactions

Kinetic parameters of the adsorption and desorption of ammonia are calculated by numerical modelling of the TPD data, whereas some parameters are taken from literature. The calculations are carried out with MATLAB® (MathWorks Inc., Natick, Massachusetts), while special functions are used for numeric solution of the equation systems as well as parameter estimation.

Estimation of free parameters, appearing within the model equations, is generated by non-linear regression. The regression analysis includes evaluation of a set of parameters for which the differences (residues) between measurands and model answers is minimised. For this purpose the MATLAB® function *lsqcurvefit* which bases upon the minimisation of the sum of residue squares under variation of kinetic parameters is used [33]. The numeric solution of the minimisation problem is based on the reflective Newton Method. For calculation of surface coverages the mass balance of gas-phase and surface adsorbed species is solved using MATLAB® function *ods*15*s* [33,34]. *ode*15*s* is a variable order multistep solver based on numerical differentiation formulas. To specify the quality of the estimated kinetic parameters their 95% confidence interval is calculated with MATLAB® function *nlparci* which involves asymptotic normal distribution.

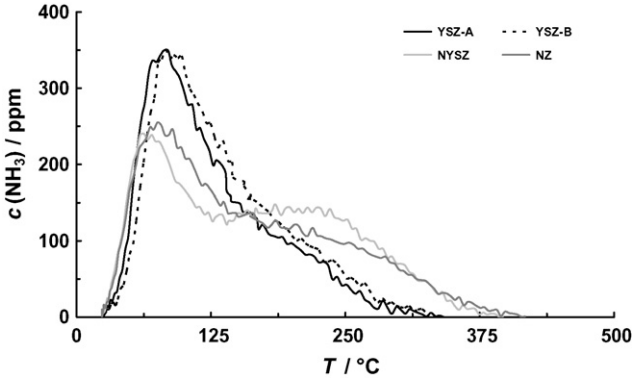

Fig. 2. NH_3 TPD patterns of the zirconia samples. Conditions: F: 1.00 l min^{-1} (STP), $\Delta T\,\Delta t^{-1}$: 15 K min^{-1}; before TPD, samples are flushed with N_2 at 25 °C and are then exposed to NH_3.

3. Results and discussion

The TPD profiles of the samples investigated are displayed in Fig. 2. In agreement with literature [35,36] the NH_3 traces exhibit an intense peak in the low-temperature range (90 °C) and a shoulder at about 230 °C, whereas the latter is pronounced for NZ and NYSZ. The desorption signals indicate two different surface species originated from the reaction of NH_3 with corresponding adsorption sites. These adsorbates are characterised by DRIFT spectroscopy. Contrary, lateral and dipole-dipole interactions discussed in [21,22,37] are considered not to be strong enough to cause splitting of the TPD patterns.

The DRIFT spectra recorded are very similar for all the samples. For simplicity only the data of NZ are shown throughout this paper. The spectrum obtained after same pre-treatment as performed in TPD, i.e. purging with N_2, exposure to NH_3 and then flushing with N_2 (each at 25 °C), is depicted in Fig. 3.

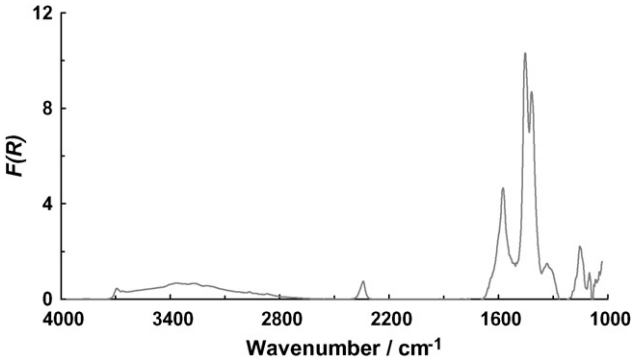

Fig. 3. DRIFT spectrum of thermally untreated NZ that was previously exposed to NH_3 (500 ppm in N_2), Conditions: F: 0.50 l min^{-1} (STP); before and after NH_3 exposure sample is flushed with N_2 at 25 °C.

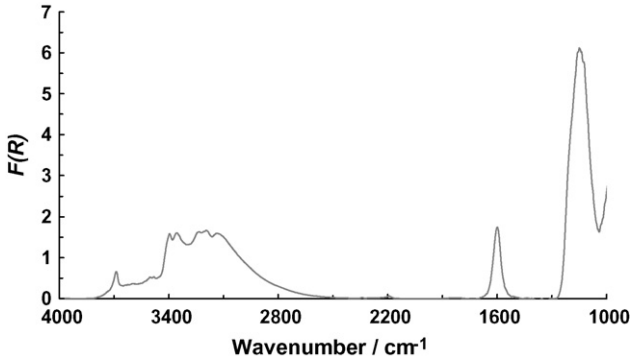

Fig. 4. DRIFT spectrum of thermally treated NZ exposed to NH_3 (500 ppm in N_2); Pre-treatment conditions: *F*: 0.50 l min^{-1} (STP); *T*: 650 °C; *t*: 60 min; before and after NH_3 exposure sample is flushed with N_2 at 25 °C.

As expected, DRIFTS bands of NH_3 species formed are observed at 1200 and ca. 1600 cm^{-1} (deformation modes) as well as in the region from 3100 to 3400 cm^{-1} (stretching modes). However, these features are not well resolved due to strong superimposition with bands related to CO_2 adsorbates, i.e. carboxylate ($\upsilon_{as}(COO^-)$: 1573 cm^{-1}; $\upsilon_s(COO^-)$: 1415 cm^{-1}) and carbonate ($\upsilon_{as}(CO_3{}^{2-})$: 1452 cm^{-1}; $\upsilon_s(CO_3{}^{2-})$: 1326 cm^{-1}; υ(C–O): 1099 cm^{-1}) [30,38–40]. The signal at 3687 cm^{-1} results from absorption of the symmetric valence vibration of bridged hydroxyl groups, which interact with two zirconium ions [30].

The strong superposition of bands of NH_3 species with that of CO_x compounds is problematic for detailed analysis of the DRIFTS data and their correlation with TPD experiments. However, thermal desorption of water and carbon dioxide adsorbates (*F*: 0.50 l min^{-1} (STP); *T*: 650 °C; *t*: 60 min) followed by NH_3 exposure at 25 °C leads to DRIFTS spectra with well defined NH_3 related bands (Fig. 4), whereby it is superiorly possible to monitor the temperature dependence of the absorbance intensities. Nevertheless, it should be taken into account that thermal desorption of H_2O and CO_2 results in a modified surface structure of the samples, e.g. a higher number of vacant Zr^{4+} sites and missing interaction of OH groups with carbonate. This has to be considered when correlating DRIFTS with TPD data.

In accordance with literature [41–47] ammonia adsorbs coordinatively onto both terminal and bridged surface hydroxyl groups ($\delta_{as}(NH_3)$: 1600 cm^{-1}; $\delta_s(NH_3)$: 1123 cm^{-1}) as well as Zr^{4+} ions ($\delta_{as}(NH_3)$: 1600 cm^{-1}; $\delta_s(NH_3)$: 1195 cm^{-1}; $\delta_s(NH_3)$: 1151 cm^{-1}). Detailed interrelation of the features at 3396, 3353, 3226, 3193 and 3133 cm^{-1} to symmetric and asymmetric stretching modes as well as overtones of the deformation modes is omitted. The accurate assignment is controversially discussed in the literature mentioned above and not crucial for the present work.

The ammonia adsorbates characterised are displayed in Fig. 5.

The adsorption onto Zr^{4+} sites occurs by overlap of the free electron pair orbital of nitrogen with the empty d_z^2 orbital of the metal ion. In contrast, the three stable N–H orbitals are too low in energy to react with the cation [30]. Savatos et al. established that the frequency of the symmetric deformation vibration of ammonia adsorbates is sensitive to the nature and charge of the metal as well as to the composition and geometry of the coordination sphere, whereas the δ_{as} vibration is not affected. The formation of the coordination complex, involving very small π backbonding from Zr^{4+} to the NH_3 ligand, enhances the force constant of the N–H bond thus increasing the frequency of the symmetric deformation vibration [43]. This effect is confirmed in the present paper as will be shown below.

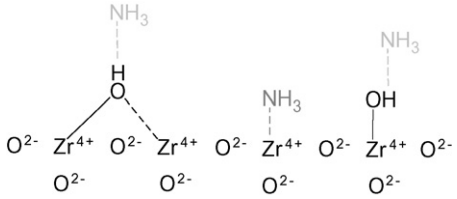

Fig. 5. Model of the surface species formed by reaction of NH_3 with ZrO_2.

Furthermore, it should be noted that ammonium species, which might be formed by interaction of Brønsted acid hydroxyl groups with NH_3 are not detected [1,44]. Therefore, we conclude that the acidity of the surface hydroxyl groups of the ziconia samples investigated is too weak to protonate NH_3.

Samples which are pre-treated at 650 °C and subsequently exposed to NH_3 at 25 °C are heated in N_2 (*F*: 0.50 l min^{-1} (STP)) to 100 °C and then to 150, 200, 250 and 350 °C to correlate DRIFTS with TPD data. Corresponding DRIFT spectra of NZ are shown in Fig. 6; as already mentioned above the spectra of the remaining samples provide analogue results.

Fig. 6(a) shows that the shoulder located at 1125 cm^{-1} disappears rapidly with increasing temperature. On the contrary, the bands of the hydroxyl groups ranging from 3650 to 3780 cm^{-1} strongly increase with temperature, whereas the feature at 3680 cm^{-1} reaches its initial intensity already at 200 °C (Fig. 6(c)).

In contrast to the band of the bridged hydroxyl species the feature of the terminal OH groups does not reappear at the original frequency but is shifted to slightly lower wavenumbers (ca. 3730 cm^{-1}). It is known from literature that hydroxyl surface groups are affected by vicinal chemisorbed ammonia species, whereas the interaction is rather weak for bridged hydroxyl species [30]. Hence, the coordination interaction of terminal hydroxyl groups with vicinal ammonia adsorbates results in broadening and delayed rise of the band at 3730 cm^{-1} as compared to the absorption signal of bridged hydroxyl groups.

The DRIFTS bands at 1151, 1195 and 1225 cm^{-1} related to δ_s vibrations of ammonia coordinated to Zr^{4+} ions decrease with increasing temperature, whereas the features at 1195 and 1225 cm^{-1} are still detectable at temperatures above 250 °C. This indicates the presence of different Lewis acid sites with specific acidity [45]. It is worth noting that the position of these signals strongly depends on the sample preparation because of the polymorphous properties of zirconia.

The signal at 1600 cm^{-1}, arising from the absorption of the asymmetric deformation modes of all NH_3 adsorbates, shows a disproportionately high decrease between 25 and 100 and 100 and 150 °C, respectively.

From the DRIFT spectra shown in Fig. 6 we derive rapid decline of the hydrogen bonded NH_3 species (δ_{as}: 1600 cm^{-1}; δ_s: 1123 cm^{-1}) between 25 and 200 °C which corresponds well to the low-temperature maximum in the TPD pattern. Contrary, the species bound to the Lewis acid Zr^{4+} sites reveal higher thermal stability indicated by the development of δ_s vibration located at 1225, 1195 and 1151 cm^{-1}. Therefore, decomposition of the latter surface component is attributed to the high temperature peak of NH_3 TPD.

Based on the TPD and DRIFTS studies a kinetic model of the adsorption and desorption of the different NH_3 surface species, which is defined by the elementary reactions (4)–(7), is constructed.

Adsorption:

$$NH_3 + Zr^{4+} \rightarrow H_3N\text{–}Zr^{4+} \quad (4)$$

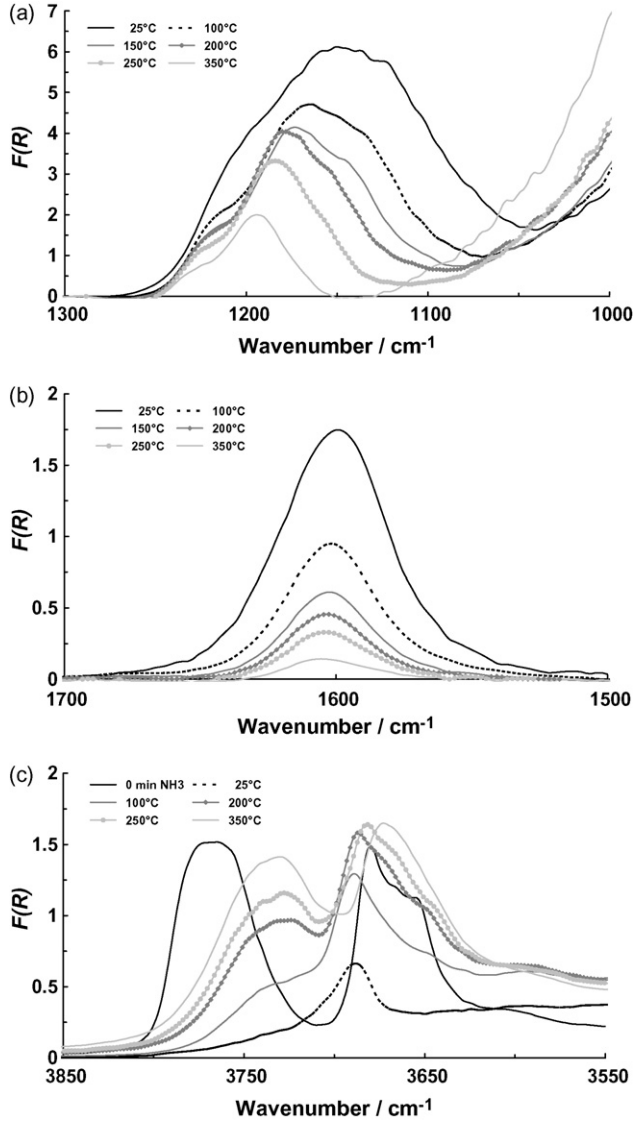

Fig. 6. DRIFT spectra of NZ after exposure to NH_3, N_2 flushing at 25 °C and subsequent thermal treatment in N_2 at 100, 150, 200, 250 and 350 °C. For clarity the figure is separated into spectral regions from 1000 to 1300 (a), 1500 to 1700 (b) and 3550 to 3850 cm^{-1} (c).

$$NH_3 + HO\text{–}Zr^{4+} \rightarrow H_3N\text{–}HO\text{–}Zr^{4+} \quad (5)$$

Desorption:

$$H_3N\text{–}Zr^{4+} \rightarrow NH_3 + Zr^{4+} \quad (6)$$

$$H_3N\text{–}HO\text{–}Zr^{4+} \rightarrow NH_3 + HO\text{–}Zr^{4+} \quad (7)$$

The rate (r_{ij}) of every reaction is described by an Arrhenius-based expression (Eq. (8)), where $E_{A,j}$ is the activation energy, R the ideal gas constant and T the temperature.

$$k_j = A_j \exp\left(-\frac{E_{A,j}}{RT}\right) \quad (8)$$

In the following section parameter indices 1 and 3 refer to adsorption and desorption of NH_3 onto Zr^{4+}sites, while indices 2, 4 are assigned to adsorption and desorption involving surface hydroxyl species.

Due to the repulsion between adsorbed species a linear decrease in activation energies (E_{A2}; E_{A4}) is assumed for desorption of ammonia with increasing NH_3 coverage. For this purpose the constants $\varepsilon_{j,\Theta}$ and $\varepsilon'_{j,\Theta}$ are introduced (Eqs. (9) and (10)); $\Theta^{Zr}_{NH_3}$ and $\Theta^{OH}_{NH_3}$ are the surface coverages of NH_3 adsorbed on Zr^{4+} sites ($NH_3^{(Zr)}$) and hydroxyl groups ($NH_3^{(OH)}$).

$$E_{A2}(\Theta_{NH_3^{(Zr)}}) = E_{A2,0}(\Theta_{NH_3^{(Zr)}})(1 - \varepsilon_{2,\Theta}\Theta_{NH_3^{(Zr)}} - \varepsilon'_{4,\Theta}\Theta_{NH_3^{(OH)}}) \quad (9)$$

$$E_{A4}\left(\Theta_{NH_3^{(OH)}}\right) = E_{A4,0}\left(\Theta_{NH_3^{(OH)}}\right) \times \left(1 - \varepsilon'_{2,\Theta}\Theta_{NH_3^{(Zr)}} - \varepsilon_{4,\Theta}\Theta_{NH_3^{(OH)}}\right) \quad (10)$$

The rates of the adsorption and desorption of $NH_3^{(Zr)}$ and $NH_3^{(OH)}$ species are described by Eqs. (11)–(14). It should be noted that a mean field approach, in which respective adsorption sites are considered to be equivalent, is used. This rather rough assumption is applied as an effective standard method designing catalytic converters and describing interactions of ammonia with metal and metal oxide surfaces [34,48,49]. In accordance to these references the present model considers free readsorption which is not in quasi-equilibrium with the desorption process. This approach is a fundamental model based on elementary reactions derived from detailed temperature dependent experiments and is generally accepted in the literature [33,34,48–53].

$$r_1 = A_1 \exp\left(-\frac{E_{A1}}{RT}\right) c_{NH_3(g)}(1 - \Theta_{NH_3^{(Zr)}}) \quad (11)$$

$$r_2 = A_2 \exp\left(-\frac{E_{A2,0}(1 - \varepsilon_{2,\Theta}\Theta_{NH_3^{(Zr)}} - \varepsilon'_{4,\Theta}\Theta_{NH_3^{(OH)}})}{RT}\right) \Theta_{NH_3^{(Zr)}} \quad (12)$$

$$r_3 = A_3 \exp\left(-\frac{E_{A3}}{RT}\right) c_{NH_3(g)}(1 - \Theta_{NH_3^{(OH)}}) \quad (13)$$

$$r_4 = A_4 \exp\left(-\frac{E_{A4,0}(1 - \varepsilon'_{2,\Theta}\Theta_{NH_3^{(Zr)}} - \varepsilon_{4,\Theta}\Theta_{NH_3^{(OH)}})}{RT}\right) \Theta_{NH_3^{(OH)}} \quad (14)$$

Kinetic modelling of the TPD profiles is based on combination of the mass balances of gaseous and adsorbed ammonia (Eqs. (15)–(17)). In accordance to the literature the analytical bench is mathematically described as a continuous stirred-tank reactor (CSTR) [4,9,33,50,54–59]. The application of the CSTR model has been shown to be a good approximation as compared to the Plug Flow Reactor (PFR) model and is therefore a widely accepted practice in numerical modelling of TPD data [60,61]. From Ref. [50] we derive that accumulation of NH_3 in the cell is negligible ($V\beta/\dot{V}T_0 < 0.02$; where V is the volume of the gas cell, β the heating rate, $\dot{V}$ the volume flow and T_0 the initial temperature). Therefore, quasi steady state conditions are assumed. The quasi steady state assumption is widely used describing TPD experiments [4,9–12,33,62].

Mass balance of gaseous ammonia in the CSTR under quasi steady state conditions:

$$\dot{V}c_{NH_3(g),\,in} - \dot{V}c_{NH_3(g),\,out} + A_{ZrO_2}\sum_{j}^{N_j}\nu_{ij}r_{ij} = 0 \quad (15)$$

Mass balance of adsorbed ammonia:

$$A_{ZrO_2}\Gamma_{ZrO_2}\beta\frac{d\Theta_{NH_3^{(Zr)}}}{dT} = A_{ZrO_2}\sum_{m}^{N_m}\nu_{nm}r_{nm} \quad (16)$$

$$A_{ZrO_2}\Gamma_{ZrO_2}\beta\frac{d\Theta_{NH_3^{(OH)}}}{dT} = A_{ZrO_2}\sum_{p}^{N_p}\nu_{op}r_{op} \quad (17)$$

$c_{NH3\,(g),in}$ and $c_{NH3\,(g),out}$ are NH_3 concentrations monitored at the reactor inlet and outlet, respectively, A_{ZrO_2} the specific surface area of the respective ZrO_2 sample, Γ_{ZrO_2} the correspondent surface concentration of active sites and ν_{ij}, ν_{nm} and ν_{op} the stoichiometric coefficients of species i, n and o of the jth, mth and pth reaction. In the TPD experiments described no additional NH_3 flow is introduced at the reactor inlet ($c_{NH3\,(g),in}$ = 0 ppm). Therefore, $c_{NH3\,(g)}$ is equal to $c_{NH3\,(g),out}$ in Eqs. (11)–(20).

The mass balance results in a system of an algebraic (Eq. (18)) and two non-linear differential equations (Eqs. (19) and (20)) by inserting Eqs. (11)–(14) in Eqs. (15)–(17).

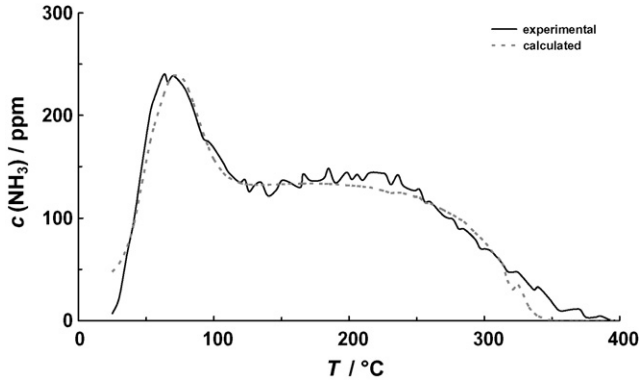

Fig. 7. Comparison of the calculated and measured NH_3 TPD profile of the sample NYSZ.

$$c_{NH_3,(g)} = \frac{A_{ZrO_2}A_2\,\exp(-E_{A2,0}(1-\varepsilon_{2,\Theta}\Theta_{NH_3^{(Zr)}}-\varepsilon'_{4,\Theta}\Theta_{NH_3^{(OH)}}/RT)\Theta_{NH_3^{(Zr)}} + A_{ZrO_2}A_4\,\exp(-E_{A4,0}(1-\varepsilon'_{2,\Theta}\Theta_{NH_3^{(Zr)}}-\varepsilon_{4,\Theta}\Theta_{NH_3^{(OH)}})/RT)\Theta_{NH_3^{(OH)}}}{\dot{V}+A_{ZrO_2}A_1\exp(-E_{A1}/RT)(1-\Theta_{NH_3^{(Zr)}})+A_{ZrO_2}A_3\,\exp(-E_{A3}/RT)(1-\Theta_{NH_3^{(OH)}})} \quad (18)$$

$$\Gamma_{ZrO_2}\beta\frac{d\Theta_{NH_3^{(Zr)}}}{dT} = A_1\,\exp\left(-\frac{E_{A1}}{RT}\right)c_{NH_3(g)}(1-\Theta_{NH_3^{(Zr)}}) - A_2\,\exp\left(-\frac{E_{A2,0}(1-\varepsilon_{2,\Theta}\Theta_{NH_3^{(Zr)}}-\varepsilon'_{4,\Theta}\Theta_{NH_3^{(OH)}})}{RT}\right)\Theta_{NH_3^{(Zr)}} \quad (19)$$

$$\Gamma_{ZrO_2}\beta\frac{d\Theta_{NH_3^{(OH)}}}{dT} = A_3\,\exp\left(-\frac{E_{A3}}{RT}\right)c_{NH_3(g)}(1-\Theta_{NH_3^{(OH)}}) - A_4\,\exp\left(-\frac{E_{A4,0}(1-\varepsilon'_{2,\Theta}\Theta_{NH_3^{(Zr)}}-\varepsilon_{4,\Theta}\Theta_{NH_3^{(OH)}})}{RT}\right)\Theta_{NH_3^{(OH)}} \quad (20)$$

This equation system is used for the evaluation of kinetic parameters by numerical modelling of the TPD data as described in Section 2.4.

Diffusion effects, which are taken into account by Delgado and Gómez [50] modelling CO_2 TPD experiments on porous materials are not considered due to the non-porous characteristics of the zirconia samples investigated. Thus, balance and differential equations used are not extended by diffusion terms, which describe pore diffusion. The influence of surface diffusion effects could additionally be investigated by kinetic Monte Carlo simulations [19–22,37,63]. However, our DRIFTS data do not provide evidence for significant transformation of one kind of adsorbate into the other.

In order to reduce the number of free parameters in the kinetic modelling procedure the preexponential factors of adsorption (A_{ads}) and desorption (A_{des}) are estimated on the basis of literature data (Table 2) [13,33,48,50,51].

In accordance to literature we consider the adsorption of NH_3 on both types of active sites as being inactivated, i.e. $E_{A1} = E_{A3} = 0$ kJ mol^{-1} [10,51]. Activation energies of the desorption reactions E_{A2} and E_{A4} as well as the constants $\varepsilon_{j,\Theta}$ are evaluated by numerical modelling. $\varepsilon'_{j,\Theta}$ is held constant (0.005) considering a minor repulsion between different surface species, i.e. $NH_3^{(Zr)}$ and $NH_3^{(OH)}$ only.

Table 2
Preexponential factors used

Preexponential factor	Value
A_{ads}	0.87 m^3 s^{-1} m^{-2}
A_{des}	1×10^{13} mol s^{-1} m^{-2}

The calculated and measured concentrations of ammonia and the corresponding coverage of NH_3 are exemplarily shown for NYSZ (Figs. 7 and 8); these results do not differ significantly from the other samples.

Fig. 7 demonstrates that the experimental NH_3 TPD profile is satisfactorily covered by the calculated data. Thus, we conclude high accuracy of our kinetic model developed. Furthermore, the calculated surface coverages indicate rapid decrease of the $H_3N\cdots\cdots HO{-}Zr^{4+}$ species, while the desorption of stronger bound NH_3 surface species starts at about 90 °C. This behaviour is in fair agreement with the DRIFTS studies described above.

Activation energies of the NH_3 desorption from uncovered ZrO_2 surfaces and constants $\varepsilon_{j,\Theta}$ determined by numerical modelling are listed in Table 3. The 95% confidence intervals shown therein indicate the reliability of the data calculated. The number of active surface sites ($N^{(Zr)}$, $N^{(OH)}$) are obtained by deconvolution of the TPD spectra using the kinetic model described above with corresponding kinetic parameters.

Activation energies calculated range from 100 to 105 and from 141 to 164 kJ mol^{-1}, respectively. These values correspond well to the scale of activation energies of desorption reactions of probe molecules which are coordinatively bound onto oxide substrates [64]. Differences between $E_{A2,0}$ and $E_{A4,0}$ are reflected in the thermal stability of the adsorbates.

Values of 95–100 kJ mol^{-1} and 128–133 kJ mol^{-1} result using Eq. (1) underlying our TPD data. These figures are close to the activation energies determined above (Table 3). It is known, that the Redhead approach often leads to unrealistically high values of energy due to the non-consideration of possible readsorption processes [9]. However, activation energies evaluated by our numerical modelling

Table 3
Number of active surface sites and calculated parameters of the desorption process

Parameter	YSZ-A	YSZ-B	NYSZ	NZ
$N^{(Zr)}$/μmol g^{-1}	12.0	13.5	71.0	88.0
$\varepsilon_{2,\Theta}$	0.27 ± 0.03	0.26 ± 0.03	0.31 ± 0.01	0.37 ± 0.02
$E_{A2,0}$/kJ mol^{-1}	141 ± 1	143 ± 1	164 ± 1	163 ± 1
$N^{(OH)}$/μmol g^{-1}	8.3	9.0	40.0	40.0
$\varepsilon_{4,\Theta}$	0.056 ± 0.013	0.067 ± 0.013	0.066 ± 0.007	0.062 ± 0.013
$E_{A4,0}$/kJ mol^{-1}	102 ± 1	105 ± 1	100 ± 1	101 ± 1

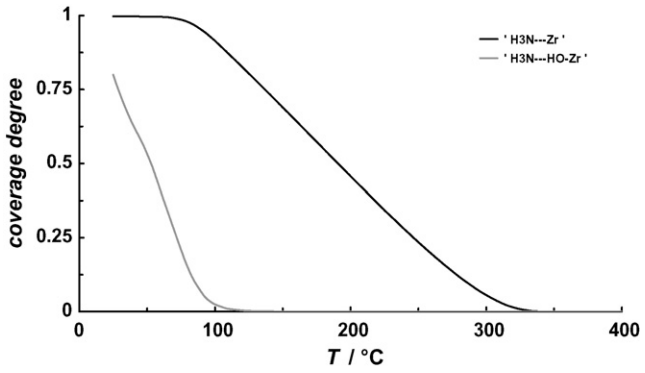

Fig. 8. Calculated NH_3 surface coverages of the sample NYSZ.

refer to zero coverage. Considering $\varepsilon_{j,\Theta}$ factors of 0.06 and 0.31 and surface coverages of 0.8 and 1, corresponding activation energies range from 95 to 100 and from 100 to 113 kJ mol^{-1} at high coverages. These values are smaller than activation energies obtained using Eq. (1).

Surface heterogeneity, i.e. adsorption onto different crystallographic faces, surface steps, edges and corners is neglected in our numerical modelling as generally done in the modelling of non-equilibrium reactions [33,34,48–53]. However, $\varepsilon_{j,\Theta}$ factors evaluated denote substantial coverage dependence of activation energies, especially for $NH_3^{(Zr)}$ adsorbates. This effect is considered to be too strong to be associated with vicinal interaction contributions only. Hence, we conclude that $\varepsilon_{j,\Theta}$ factors imply both energetic heterogeneity of ZrO_2 surfaces and repulsion forces of NH_3 species. Therefore, the model presented is not only an effective tool determining activation energies of desorption reactions but also provides a measure for describing surface heterogeneity. Evaluated $\varepsilon_{j,\Theta}$ factors of 0.06 and 0.31 (Table 3) implicate that $NH_3^{(Zr)}$ adsorbates are effected much stronger by vicinal interactions and surface heterogeneity than $NH_3^{(OH)}$ species.

Additionally, surface heterogeneity could be quantitatively addressed by continuous energy distributions based on quasi-equilibrium approaches evaluating adsorption enthalpies [9–12].

The, in dependence of the amount of adsorbed $H_3N\cdots Zr^{4+}$ species, increasing activation energy is ascribed to sample dependent proportions of surface carboxylate and carbonate species and superimposed surface heterogeneity effects. CO_x adsorbates block high energy surface sites and – according to the interaction model of Nakano et al. and Chuah et al. – execute a repulsive interaction onto NH_3 species [35,65].

4. Conclusion

Numerical modelling of the adsorption and thermal desorption of NH_3 on ZrO_2 surfaces provided activation energies of the desorption reactions between 100 and 105 kJ mol^{-1} and from 141 to 163 kJ mol^{-1}. These are associated to ammonia species adsorbed coordinatively onto surface hydroxyl groups ($H_3N\cdots\cdots HO–Zr^{4+}$) and Zr^{4+} ions ($H_3N\cdots\cdots Zr^{4+}$), respectively. The study shows that combined DRITFS and TPD analysis are an effective approach characterising surface adsorbed species, deriving elementary reactions and determining corresponding kinetic parameters as well as describing surface heterogeneity.

References

[1] G. Ertl, J. Weitkamp, H. Knözinger, Handbook of Heterogeneous Catalysis, 4, first ed., Wiley-VCH, Weinheim, 1997.
[2] N. Apostolescu, B. Geiger, K. Hizbullah, M.T. Jan, S. Kureti, D. Reichert, F. Schott, W. Weisweiler, Appl. Catal. B 62 (2006) 104–114.
[3] C. Kenney, Y. Maharn, A.E. Nelson, Thermochim. Acta 434 (2005) 55–61.
[4] W. Makowski, Thermochim. Acta 454 (2007) 26–32.
[5] A. Gerasini, A. Auroux, J. Therm. Anal. 37 (1991) 1737–1744.
[6] A. Auroux, J.C. Védrine, Stud. Surf. Sci. Catal. 20 (1985) 311–318.
[7] A. Auroux, M.L. Occelli, Stud. Surf. Sci. Catal. 84 (1994) 693–699.
[8] M. Muscas, V. Solinas, S. Gontier, Stud. Surf. Sci. Catal. 94 (1995) 101–107.
[9] J.M. Kanervo, K.M. Reinikainen, A.O.I. Krause, Appl. Catal. A 258 (2004) 135–144.
[10] J.M. Kanervo, T.J. Keskitalo, R.I. Slioor, A.O.I. Krause, J. Catal. 238 (2006) 382–393.
[11] T. Panczyk, W. Gac, M. Panczyk, T. Borowiecki, W. Rudzinski, Langmuir 22 (2006) 6613–6621.
[12] T.J. Keskitalo, M.K.V. Niemelä, A.O.I. Krause, Langmuir 23 (2007) 7612–7619.
[13] P.A. Redhead, Vacuum 12 (1962) 203–211.
[14] A.W. Smith, S. Aranoff, J. Phys. Chem. 62 (1958) 684–686.
[15] G. Ehrlich, J. Appl. Phys. 32 (1961) 4–15.
[16] S. Sato, N. Ichikawa, T. Sodesawa, J. Mol. Catal A: Chem. 256 (2006) 106–112.
[17] J.A. Konvalinka, P.H. Scholten, P.H. van Oeffelt, Appl. Catal. 1 (1981) 141–158.
[18] S. Smeds, T. Salmi, L.P. Lindfors, O. Krause, Appl. Catal. A 144 (1996) 177–194.
[19] V.P. Zhdanov, T. Matsushima, Surf. Sci. 583 (2005) 253–264.
[20] V.P. Zhdanov, T. Matsushima, Surf. Sci. 601 (2007) 2373–2377.
[21] K.A. Fichthorn, W.H. Weinberg, J. Chem. Phys. 95 (1991) 1090–1096.
[22] H.C. Kang, W.H. Weinberg, Chem. Rev. 95 (1995) 667–676.
[23] G. Scheying, Ph.D. Thesis, University of Darmstadt, 1998.
[24] T. Finke, M. Gernsbeck, U. Eisele, H. Bockhorn, S. Kureti, M. Hartmann, C. Vincent, cfi/Ber. DKG 84 (2007) 24–29.
[25] H.G. Ang, K.S. Chan, G.K. Chuah, S. Jaenicke, S.K. Neo, J. Chem. Soc. Dalton Trans. (1995) 3753–3758.
[26] S. Sato, K. Takematsu, T. Sodesawa, F. Nozaki, Bull. Chem. Soc. Jpn. 65 (1992) 1486–1490.
[27] S. Sato, K. Koizumi, F. Nozaki, J. Catal. 178 (1998) 264–274.
[28] N. Katada, M. Niwa, Catal. Surveys Jpn. 1 (1997) 215–226.
[29] V.A. Pokrovskiy, J. Therm. Anal. Calorim. 62 (2000) 407–415.
[30] A.A. Davydov, Molecular Spectroscopy of Oxide Catalyst Surfaces, first ed., John Wiley & Sons, Chichester, 2003.
[31] E.H. Korte, Analytiker Taschenbuch, first ed., Springer, Berlin, 1990.
[32] W. Gottwald, G. Wachter, IR-Spektroskopie für Anwender, first ed., Wiley-VCH, Weinheim, 1997.
[33] M. Crocoll, S. Kureti, W. Weisweiler, J. Catal. 229 (2005) 480–489.
[34] L. Olsson, B. Westerberg, H. Persson, E. Fridell, M. Skoglundh, B. Andersson, J. Phys. Chem. B 103 (1999) 10433–10439.
[35] G.K. Chuah, S. Jaenicke, T.H. Xu, Surf. Interface Anal. 28 (1999) 131–134.
[36] S. Sato, N. Ichikawa, T. Sodesawa, J. Mol. Catal. A: Chem. 256 (2006) 106–112.
[37] V.P. Zhdanov, B. Kasemo, Surf. Rev. Lett. 5 (1998) 551–558.
[38] G. Busca, V. Lorenzelli, Mater. Chem. Phys. 7 (1982) 89–126.
[39] C. Morterra, S. Coluccia, G. Ghiotti, A. Zecchina, Z. Phys. Chem. 104 (1977) 275–290.
[40] M. Primet, P. Pichat, M.V. Mathieu, J. Phys. Chem. 75 (1971) 1221–1226.
[41] A.A. Davydov, Infrared Spectroscopy of Adsorbed Species on the Surface of Transition Metal Oxides, first ed., John Wiley & Sons, Chichester, 1990.
[42] A.A. Tsyganenko, J. Mol. Struct. 29 (1975) 299–318.
[43] G.F. Savatos, D.M. Sweeny, S. Mizushima, S. Curran, J.V. Quaglinana, J. Am. Chem. Soc. 79 (1957) 3313–3315.
[44] N. Naito, N. Katada, M. Niwa, J. Phys. Chem. B 103 (1999) 7206–7213.
[45] V.N. Filimonov, Y. Lopatin, N. Shukhov, Kinet. Katal. 10 (1969) 458–464.
[46] N. Yamamoto, S. Sato, R. Takahashi, K. Inui, J. Mol. Catal. A: Chem. 243 (2006) 52–59.
[47] B.-Q. Xu, T. Yamaguchi, Acta Phys. -Chim. Sin. 11 (1995) 337–341.

[48] L. Lietti, I. Nova, S. Camurri, E. Tronconi, P. Forzatti, AIChE J. 43 (10) (1997) 2559–2570.
[49] D. Chatterjee, T. Burghardt, M. Weibel, I. Nova, A. Grossale, E. Tronconi, SAE World Congress (2007) 2007-01-1136.
[50] J.A. Delgado, J.M. Gómez, Langmuir 21 (2005) 3503–3510.
[51] Y. Chen, J.A. Dumesic, T. Slabiak, H. Topsøe, N.-Y. Topsøe, J. Catal. 163 (1996) 409–417.
[52] R. Quicemo, O. Deutschmann, J. Warnatz, J. Pérez-Ramírez, Catal. Today 119 (2007) 311–316.
[53] D. Chatterjee, O. Deutschmann, J. Warnatz, Faraday Discuss. 119 (2001) 371–384.
[54] W. Makowski, D. Majda, J. Porous Mater. 14 (2007) 27–35.
[55] H.Y. Lin, Y.W. Chen, Thermochim. Acta 419 (2004) 283–290.
[56] R.J. Cvetanovic, Y. Amenomiya, Catal. Rev. 6 (1972) 21–48.
[57] P.I. Lee, J.A. Schwarz, J. Catal. 73 (1982) 272–287.
[58] J.M. Zowtiak, C.H. Bartholomew, J. Catal. 83 (1983) 107–120.
[59] R.A. Gemmin, R.J. Gorte, J. Catal. 90 (1984) 32–39.
[60] O. Hinrichsen, F. Rosowski, M. Muhler, G. Ertl, Stud. Surf. Sci. Catal. 109 (1997) 389–400.
[61] O. Hinrichsen, A. Hornung, M. Muhler, Chem. Eng. Technol. 22 (1999) 1039–1042.
[62] J.P. Joly, A. Perrard, Langmuir 17 (2001) 1538–1542.
[63] V.P. Zhdanov, Surf. Rev. Lett. 5 (1998) 977–981.
[64] S. Kureti, Ph.D. Thesis, University of Karlsruhe, 2000.
[65] Y. Nakano, T. Iizuka, H. Hattori, K. Tanabe, J. Catal. 57 (1979) 1–10.